*J. Fluid Mech.* (1990), *vol.* 217, *pp.* 575–593
*Printed in Great Britain*



# Flow in curved ducts. Part 2. Rotating ducts

By P. DASKOPOULOS AND A. M. LENHOFF†
Department of Chemical Engineering, University of Delaware, Newark, DE 19716, USA

(Received 25 August 1989)

When a coiled tube is rotated about the coil axis, the effects of rotation interact with centrifugal and viscous effects to complicate the flow characteristics beyond those seen in stationary curved ducts. The phenomena encountered are examined for steady, fully developed Newtonian flow in circular tubes of small curvature. The governing equations are solved using orthogonal collocation, and the results presented cover both the nature of the flow and the bifurcation structure. When rotation is in the same direction as the axial flow imposed by a pressure gradient, the flow structure remains similar to that seen in stationary ducts, i.e. with two- or four-vortex secondary flows in addition to the axial flow. There are, however, quantitative changes, which are due to the Coriolis forces resulting from rotation. The bifurcation structure also shows only quantitative changes from that for stationary ducts at all values of Taylor number examined. More complex behaviour is possible when rotation opposes the flow due to the pressure gradient. In particular, the direction of the secondary flow may be reversed at higher rotational strengths, and the mechanism of the flow reversal is explored. The flow reversal occurs smoothly at low Taylor numbers, but at higher rotational strengths a cusp appears in the primary solution branch in the vicinity of the flow reversal.

## 1. Introduction

In a previous paper (Daskopoulos & Lenhoff 1989, hereinafter referred to as I), we discussed the bifurcation characteristics for developed flow in stationary curved ducts. The work presented here deals with rotating curved ducts, which are relevant to systems involving helically or spirally coiled tubes rotating about the coil axis. Such systems are encountered in applications such as separation processes (Adler *et al.* 1981, 1982; Lennartz, Gorensek & Adler 1987) and cooling devices in rotary machines such as gas turbines, electric generators, motors, etc.

The principles of rotation in pipe flow and the roles of centrifugal and Coriolis forces have been studied extensively (see e.g. Batchelor 1967; Greenspan 1968), but although the underlying physical phenomena are well understood, rotating curved pipes have not been examined in detail. The nature of the flow is affected by the interaction of the imposed pressure-driven axial flow and system rotation, with the rotation introducing additional parametric dependence beyond that encountered for stationary curved ducts, and Coriolis forces becoming important in addition to just centrifugal effects.

The effects of rotation alone have been studied in the case of a straight pipe rotating about an axis perpendicular to the pipe axis, a limiting case of the more general situation of flow in rotating curved pipes. Flow in rotating straight ducts is of interest also because the secondary flows that arise here are qualitatively similar

† Author to whom correspondence should be addressed.

to those in stationary curved systems, in view of the similar centrifugal mechanisms inducing the secondary flows in the two systems. Thus a brief overview of flow in rotating straight pipes is provided.

To describe behaviour in the limit of low rotational speeds, Barua (1954) used a regular perturbation expansion about the Poiseuille flow limit, similar to Dean's (1927, 1928) approach for stationary curved duct flow. Results qualitatively similar to Dean's were obtained: a secondary flow consisting of a pair of counter-rotating helical vortices, and an increase in the friction factor ratio. Subsequent boundary-layer analyses also predicted a significant increase in the friction factor with rotational speed for small rotational rates and high axial pressure gradients (Mori & Nakayama 1968; Itō & Nanbu 1971), the latter group also obtaining satisfactory agreement with their experimental measurements. Mansour (1985) used a computer extension of the perturbation expansion in seeking results at higher angular velocities, in the spirit of Van Dyke's (1975) method applied to flow in stationary curved pipes (Van Dyke 1978). However, the applicability of the results far beyond the Poiseuille limit is questionable.

In the limit of rapid rotation compared to the axial flow, a geostrophic core surrounded by a thin boundary layer at the wall can be assumed (Benton & Boyer 1966); the analogous situation in stationary curved ducts is that of high Dean numbers (Barua 1963), and similar results are obtained for both problems. Jones & Walters (1967) also adapted an analysis of high-Dean-number flow in stationary curved ducts (Dean & Hurst 1959) to high-rotation-rate flow in straight tubes.

For the situation of comparable rotation and imposed axial flow, numerical solutions of the describing equations are required. Speziale's (1982) work on ducts of rectangular cross-section revealed a structure for the secondary flow very similar to that subsequently observed in stationary curved ducts (Winters 1987; I). The usual counter-rotating double-vortex configuration for the secondary flow was seen in the limit of slow rotation, but with a substantial increase in rotational speed at sufficiently high Reynolds numbers, this configuration breaks down into an asymmetric four-vortex configuration. With a further increase in rotational speed, the original picture of double counter-rotating vortices reappears. These initial studies of bifurcation phenomena were extended, and stability of the solutions examined, by Kheshgi & Scriven (1985), for rotating ducts of square cross-section. They also reported the existence of multiple solutions, exhibiting two- and four-vortex structures symmetric with respect to the centreline of the duct. These two branches were found to be stable, and joined by an unstable solution branch that develops through two turning points.

Flows in stationary curved and rotating straight conduits are thus qualitatively similar, but the combined effects of curvature and rotation, relevant to flow in rotating curved ducts, have not been explored thoroughly. The initial work (Ludwieg 1951; Hocking 1967) used the momentum-integral method to solve the boundary-layer equations for large values of Dean number and rotational velocity, and suggested a significantly higher pressure drop than that for stationary systems. At lower flow and rotation rates, Miyazaki's (1971, 1973) solution also predicted an increase of the friction factor with an increase in the strength of rotation. The flow here is characterized by a secondary flow consisting of a pair of counter-rotating vortices, qualitatively similar to the picture in other systems described above. However, since Miyazaki considered only the case where the rotation and the pressure-driven flow through the duct are in the same direction, he left part of the parameter space unexplored.

Itō & Motai (1974) realized that while centrifugal forces act radially outwards

irrespective of the direction of rotation of the pipe, the Coriolis force is perpendicular to both the axis of rotation and the direction of the relative velocity of the fluid, and acts radially outwards or inwards for positive or negative rotation respectively. Their calculations with opposing rotation and axial flow directions revealed a reduction of the strength and even a reversal of the direction of the secondary flows, the reversal occurring where the effects of centrifugal and Coriolis forces just neutralize each other. The secondary flow exhibits a four-vortex character, qualitatively and quantitatively different from the four-vortex solution observed in stationary ducts and discussed in I. A further increase in the relative magnitude of rotation leads to the disappearance of the four-vortex structure and reversal of the circulation pattern of the secondary flow, while an increase of the axial flow strength leads back to the familiar two-vortex secondary flow pattern observed in stationary curved ducts.

Itō & Motai's results were obtained using a perturbation expansion and are thus limited to relatively small Dean numbers. Menon (1984) confirmed the reversal of the secondary flow even for higher Dean numbers, but since he did so by modifying Van Dyke's (1978) analysis, based on numerical extension of a perturbation expansion, his results are not definitive. Joseph & Adler (1975) also observed the secondary flow reversal for flow in helically coiled tubes of square cross-section oscillating sinusoidally about the helix axis.

Experimental studies in rotating circular (Eutenеuer & Piesche 1978) and rectangular curved ducts (Ludwieg 1951; Piesche & Felsch 1980; Piesche 1982) have confirmed that the pressure drop is significantly higher than that for straight pipes, in agreement with theoretical studies.

Although the qualitative nature of flow in rotating curved ducts has been elucidated, a complete description of laminar flow over the entire parameter space remains to be obtained. In particular, the bifurcation structure and the mechanism of secondary flow reversal need to be explained further. These issues are addressed in this paper.

## 2. Problem formulation and solution

The specific idealized problem considered in I was developed, incompressible, Newtonian flow in a curved tube of small curvature and negligible pitch, the driving force being a pressure gradient $G$. The additional feature, rotation, can be incorporated in either of two ways: modification of the wall boundary condition while leaving the describing equations unchanged, or use of a rotating coordinate system, which would leave the boundary conditions unchanged but affect the describing equations. The latter approach was preferred because it allowed the solution procedure used in I to be implemented directly. The modified coordinate system is the same orthogonal toroidal one as used in I (figure 1), but it rotates at angular velocity $\omega$. The effect of rotation is to introduce a fictitious body force (see e.g. Greenspan, 1968), which gives rise to an additional contribution $\frac{1}{2}\rho\omega^2(R+r'\cos\alpha)^2$ to the pressure.

The resulting equations in the limit of small curvature are, in dimensionless form,

$$\nabla^2 w+\frac{1}{r}\left(\frac{\partial\psi}{\partial r}\frac{\partial w}{\partial\alpha}-\frac{\partial\psi}{\partial\alpha}\frac{\partial w}{\partial r}\right)=-D+\delta Ta\left(\sin\alpha\frac{\partial\psi}{\partial r}+\frac{\cos\alpha}{r}\frac{\partial\psi}{\partial\alpha}\right), \tag{1}$$

$$\nabla^4\psi+\frac{1}{r}\left(\frac{\partial\psi}{\partial r}\frac{\partial}{\partial\alpha}-\frac{\partial\psi}{\partial\alpha}\frac{\partial}{\partial r}\right)\nabla^2\psi=-(w+\tfrac{1}{2}Ta)\left(\sin\alpha\frac{\partial w}{\partial r}+\frac{\cos\alpha}{r}\frac{\partial w}{\partial\alpha}\right), \tag{2}$$

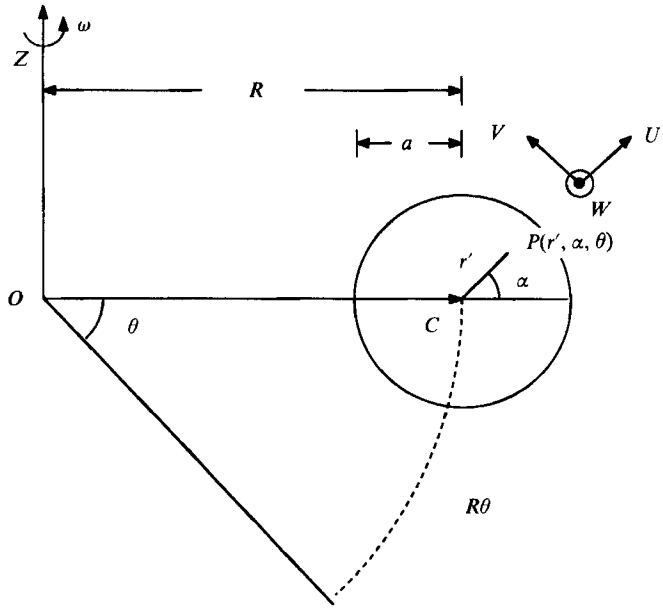


FIGURE 1. Rotating toroidal coordinate system.

where radial position and the $(r', \alpha, \theta)$-components of velocity, $(U, V, W)$, are scaled as

$$r = \frac{r'}{a}, \quad u = \frac{aU}{\nu}, \quad v = \frac{aV}{\nu}, \quad w = \frac{aW}{\nu}\left(\frac{2a}{R}\right)^{\frac{1}{2}}, \tag{3}$$

with $\nu$ the kinematic viscosity. Equations (1) and (2) are written in terms of the dimensionless secondary flow stream function $\psi(r, \alpha)$ instead of the secondary flow velocities $u$ and $v$. The key dimensionless parameters are the Dean number

$$D = \frac{Ga^3}{\mu\nu}\left(\frac{2a}{R}\right)^{\frac{1}{2}} \tag{4}$$

and the Taylor number

$$Ta = 2(2\delta)^{\frac{1}{2}}\frac{\alpha\omega R}{\nu}, \tag{5}$$

where $\mu$ is the dynamic viscosity. Alternative scaling approaches would lead to different dimensionless parameters, e.g. a Rossby number ($\sim D/Ta$) or an Ekman number ($\sim 1/Ta\delta^{\frac{1}{2}}$). The particular dimensionless parameters used in this work lead to an explicit dependence of one term in equation (1) on the curvature $\delta = a/R$. This term is of order $\delta$ in a slowly rotating system and can be ignored in the limit of small curvature, but since it can become significant for very fast rotation, it must be retained in the system equations. Because including $\delta$ as an independent parameter significantly increases the scope of the problem, the numerical simulations reported later are based on using the fixed value $\delta = 0.01$ as typical of small curvature. Choosing a different value for $\delta$ has little effect when rotation is weak ($Ta \ll D$), and while quantitative results are affected at higher rotational speeds, the physical picture is not changed (Daskopoulos 1989).

Equations (1) and (2) for $Ta = 0$ reduce to the equations for stationary systems used in I, and in the limit $\delta = 0$, after proper scaling, to the equations for flow in a straight pipe rotating about a perpendicular axis (Mansour 1985).

As was the case in I, the only solutions examined are those that are symmetric about the centreline of the tube. In view of this and the use of a rotating coordinate system, the boundary conditions used in I for stationary ducts apply here too. This has the advantage that the orthogonal collocation technique used to solve the equations in I can be used here with the same basis functions, viz. Chebyshev polynomials and Fourier series in the radial and azimuthal directions respectively. The resulting set of algebraic equations was solved, as in I, using Newton's method, with the convergence criterion that the fractional improvement between successive iterations be less than $10^{-12}$, based on the $\infty$-norm.

The bifurcation structure presented in I for stationary curved ducts was obtained by continuation in $D$, with additional insight into the morphogenesis obtained by continuation from the 'perfect' problem (Benjamin 1978) of azimuthal flow in a curved slit. The structure has a stable primary solution, characterized by a two-vortex secondary flow, as the unique solution for small $D$, and present for all $D$ in the laminar flow regime. A one-sided bifurcation at $D \doteq 956$ introduces two four-vortex solutions, one stable and the other unstable, also existing over the remainder of the laminar flow regime. A new solution family comprising two unstable branches was also found above a turning point at $D \doteq 2494$.

The approach used here to include $Ta$ as an additional parameter is continuation in $Ta$, starting from the $Ta = 0$ limit examined in I, a situation summarized in the previous paragraph. Zeroth- and first-order continuation techniques were used, with singular points traversed by arclength continuation (Keller 1977, 1982). It is also possible to study the morphogenesis of the bifurcation structure by starting from the perfect problem, in this case combined pressure-driven azimuthal flow and rotation in a curved slit, but such an investigation is much more demanding computationally and was not undertaken.

The stability of the different solutions was determined by examining the eigenvalues of the Jacobian matrix, as described in I.

## 3. Results and discussion

Because of the definition of $\omega$, $Ta > 0$ represents the case of positive rotation, i.e. rotation in the same sense as the fluid flow due to the axial forcing, and $Ta < 0$ that of negative rotation. Because of the physical differences between the two situations, first examined by Itō & Motai (1974), the results for $Ta > 0$ and $Ta < 0$ are discussed separately. Additional details are presented by Daskopoulos (1989).

### 3.1. *Codirectional rotation and axial flow*

For slow rotation, the results obtained for both the bifurcation structure and the flow characteristics are essentially identical to those for stationary ducts described in I. As $Ta$ is increased, the flow characteristics remain qualitatively the same, but there are quantitative changes: the secondary flow is significantly enhanced and the primary flow becomes weaker. These effects are visible in the axial velocity contours and secondary flow streamlines (figure 2*a*, *b*) and the axial and radial velocities along the centreline (figure 3) for the primary solution at $D = 100$. The values of axial velocity are relative to the tube wall, because of the use of the rotating coordinate system, and a negative value of $r$ in figure 3 indicates values along the line $\alpha = \pi$. The

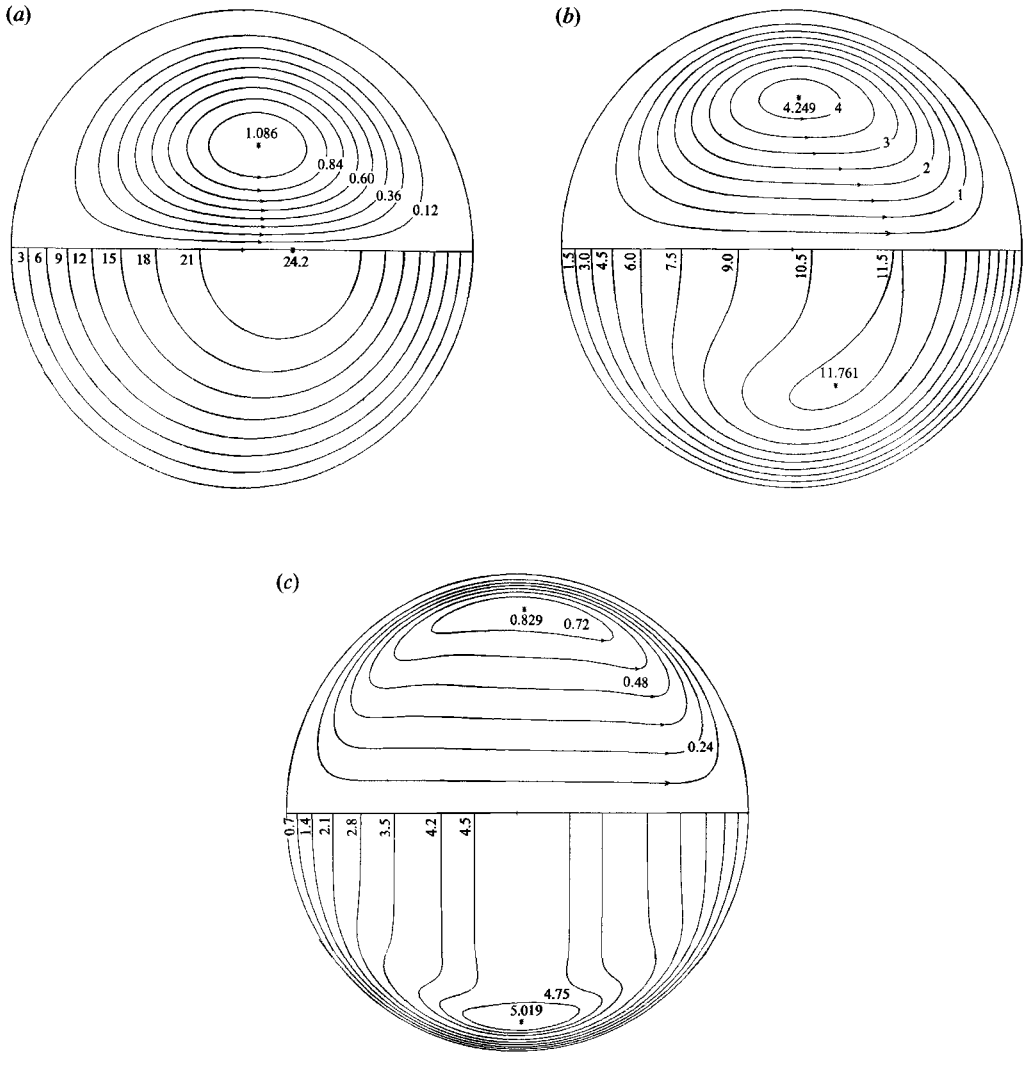


FIGURE 2. Secondary flow streamlines (top) and axial velocity contours (bottom) for stable two-vortex solution at $D = 100$. (*a*) $Ta = 1$; (*b*) $Ta = 1000$; (*c*) $Ta = 10000$.

changes seen can be explained in terms of Coriolis forces, which become significant as the rotational speed increases. The component in the cross-section is directed towards the outer wall of the tube and hence enhances the secondary flow, while the axial component, proportional to the secondary flow velocity, opposes the axial flow in the central core of the tube, and hence decelerates the main flow. This argument does not hold near the upper wall of the tube, where the secondary flow is inward.

When the Taylor number is high enough for rotation to be dominant, a totally different flow situation is obtained, as shown for the primary solution family in figure 2(*c*), with similar distortion also observed in the additional solution families. In general the effects of dominant rotation are manifested by Ekman boundary layers developing near the walls, with a geostrophic central core of the fluid displaying inviscid behaviour. This situation resembles that described by Benton & Boyer (1966) for flow through a rapidly rotating straight pipe, and it is a characteristic

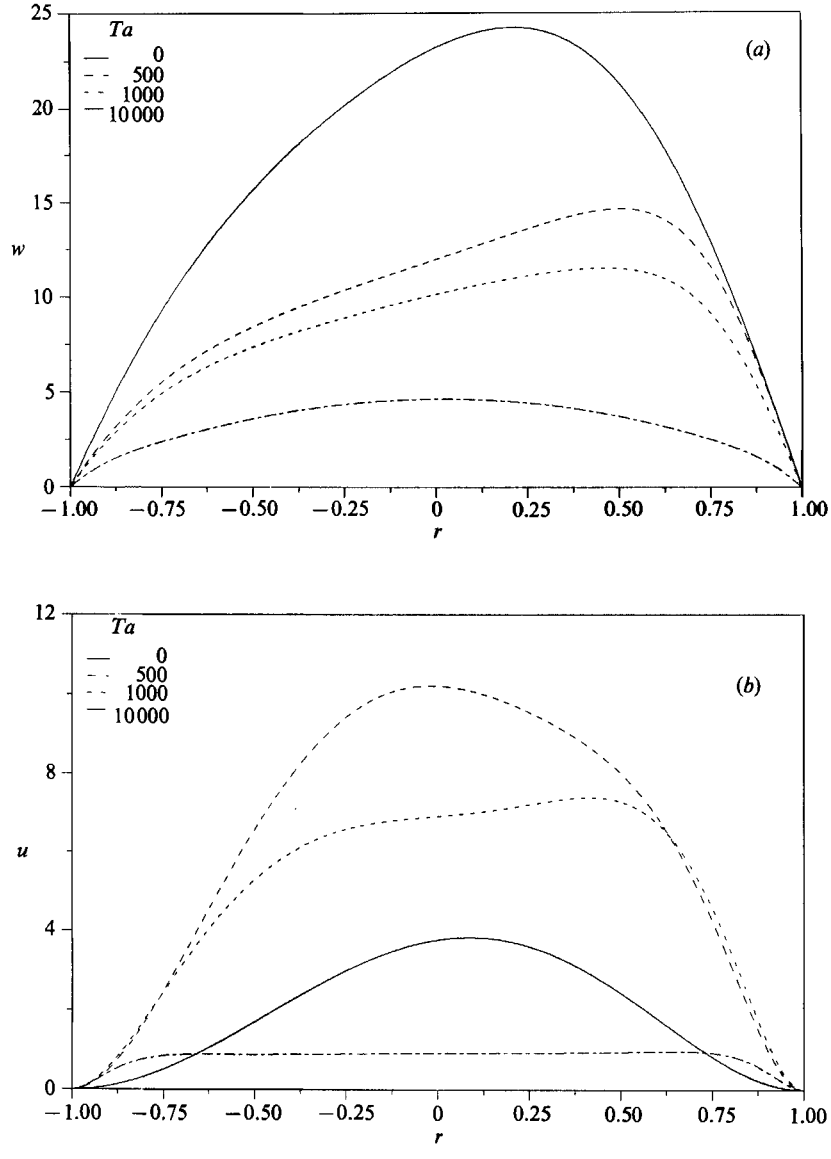


FIGURE 3. (*a*) Axial and (*b*) radial velocity distributions along the centreline at $D = 100$.

Taylor–Proudman flow configuration (Greenspan 1968) with columnar motion in the central core: entire pillars of fluid in the direction parallel to the axis of rotation move axially at a constant velocity, while the flow in the core in the direction parallel to the rotation axis becomes minimal, as indicated by the parallel axial isovels and the flattening of the secondary flow streamlines. The initial increase in strength of the secondary flow is replaced by a weakening, because the deceleration of the axial flow leads to weaker centrifugal forces. Both the axial velocity contours and the secondary flow streamlines exhibit symmetry about the vertical centreline, in accordance with the observation that in general Coriolis forces tend to restore the equilibrium state of the system (Greenspan 1968). The axial velocity at the edge of

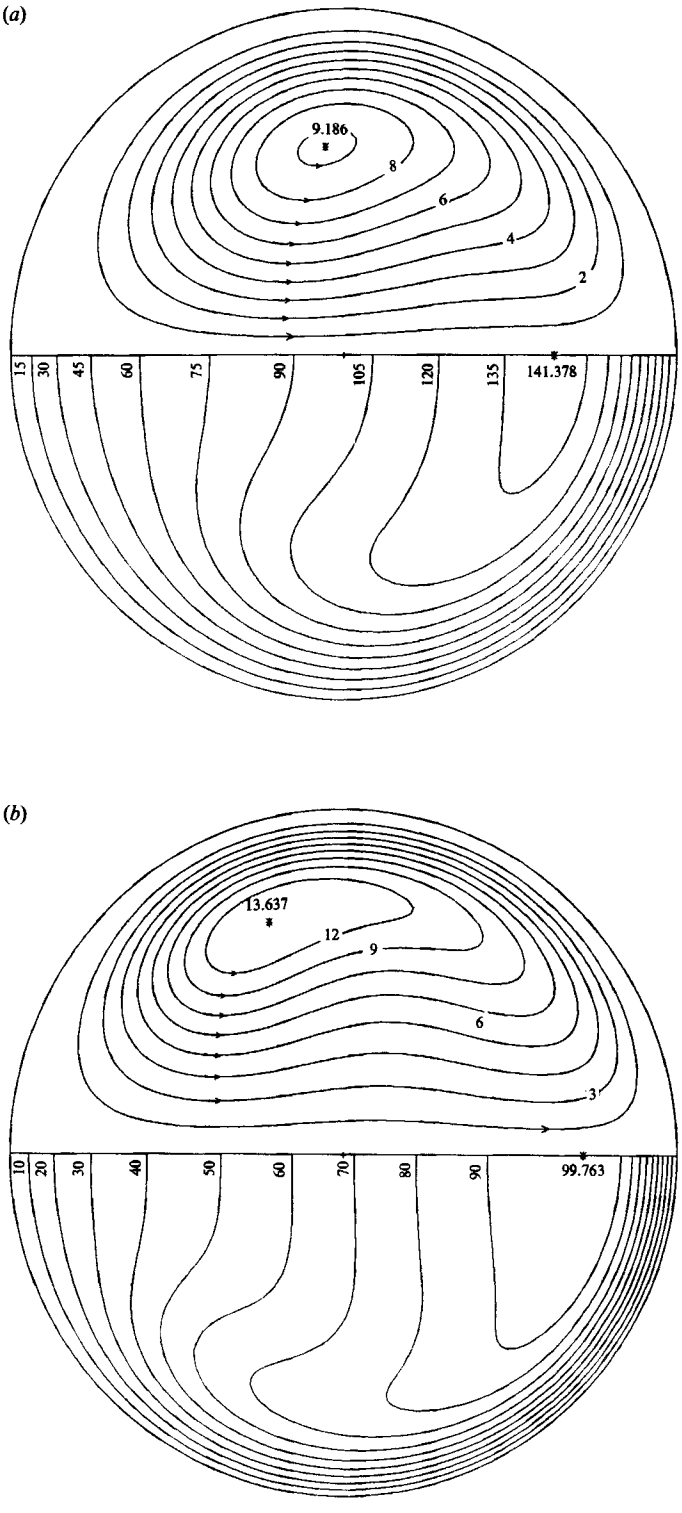


FIGURE 4. Secondary flow streamlines and axial velocity contours for stable two-vortex solution at $D = 1000$. (*a*) $Ta = 1$; (*b*) $Ta = 1000$.

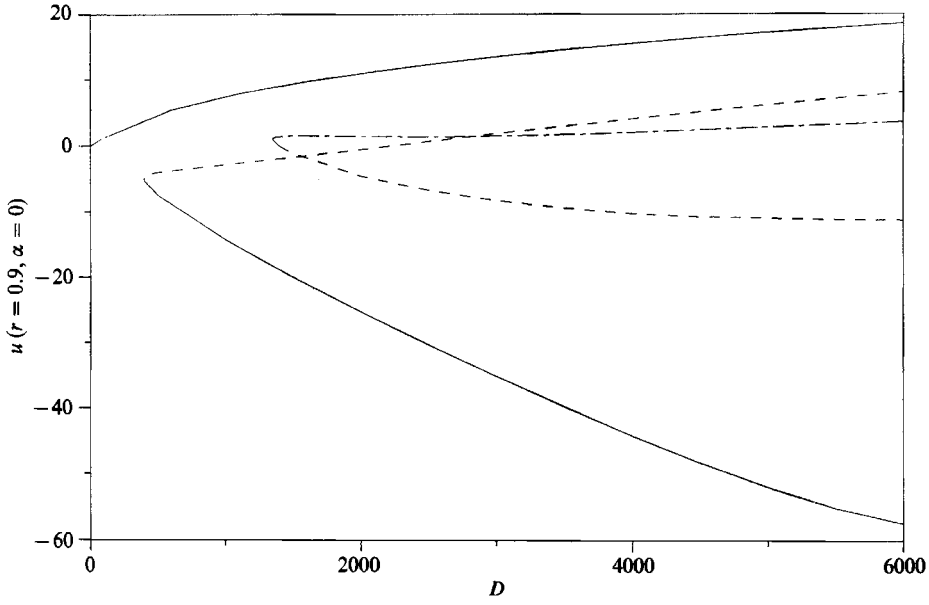


FIGURE 5. Bifurcation diagram at $Ta = 1000$, with radial velocity at $r = 0.9$ on plane of symmetry as state variable. ——, Stable solution; ——, unstable solution; ———, doubly unstable solution.

| $Ta$ | $D_1$ | $D_2$ |
|---|---|---|
| 0 | 955.73 | 2494.22 |
| 1 | 954.08 | 2490.17 |
| 10 | 939.06 | 2487.06 |
| 100 | 800.66 | 2348.72 |
| 500 | 478.27 | 1774.47 |
| 750 | 419.80 | 1525.87 |
| 1000 | 401.43 | 1352.93 |
| 2500 | 492.38 | 1027.76 |
| 5000 | 774.48 | 1178.74 |
| 7500 | 1100.12 | 1491.79 |
| 10000 | 1458.00 | 1880.41 |

TABLE 1. Turning points for the case of positive rotation

the Ekman layer at the lateral walls ($\alpha = \pm\frac{1}{2}\pi$) shows an overshoot, as has also been observed experimentally by Hart (1971) for rotating rectangular geometries.

The effects of rotation illustrated for $D = 100$ in figure 2 are less pronounced at higher $D$. Figure 4, for example, shows values of $Ta$ up to 1000 to induce quantitative but not appreciable qualitative changes at $D = 1000$. A reasonable measure of whether rotation is significant is that $Ta$ should exceed $D$ in magnitude.

The bifurcation structure remains qualitatively the same as that presented in I for stationary ducts, although there are quantitative differences corresponding to the trends described above. An example is shown in figure 5 for $Ta = 1000$. Initially the solutions other than the primary one are stabilized by rotation, as indicated by a shift of the turning points to lower values of $D$ as $Ta$ increases. However, this trend is reversed in the limit of dominant rotation, with the turning points moving back towards higher values of $D$ as $Ta$ is increased further. The positions of the turning points over the entire parameter range of positive $Ta$ are given in table 1. $D_1$ denotes

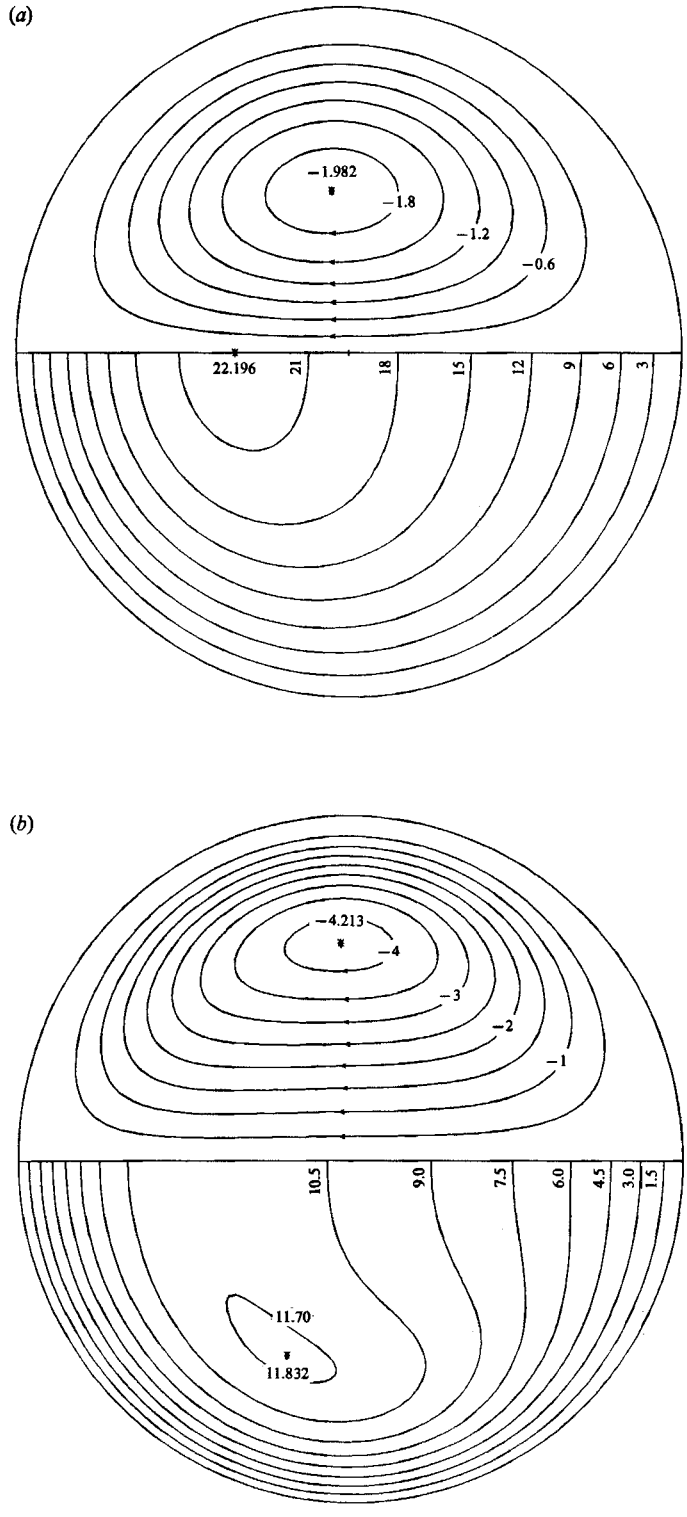


FIGURE 6. Secondary flow streamlines and axial velocity contours for stable two-vortex solution at $D = 100$. (*a*) $Ta = -100$; (*b*) $Ta = -1000$.

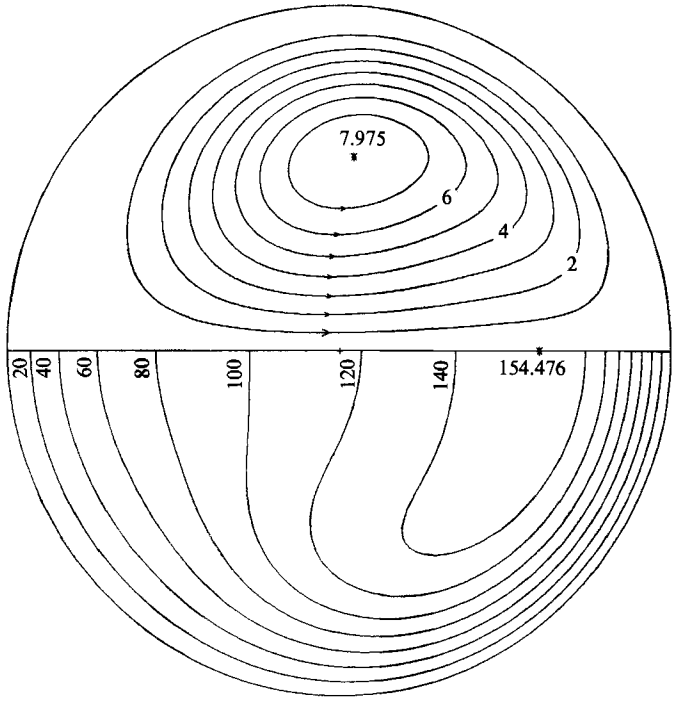


FIGURE 7. Secondary flow streamlines and axial velocity contours for stable two-vortex solution at $D = 1000$, $Ta = -100$.

the turning point between the stable and unstable four-vortex branches and $D_2$ the corresponding one for the additional solution family. The reversal of the movement from smaller to larger values of $D$ does not happen in the same region for the two turning points. This is to be expected, since the flow nature depends on the relative magnitude of the effects arising from the pressure-driven axial flow and the rotation. Hence, for lower values of $D$ the rotation-dominated region begins at lower values of $Ta$.

### 3.2. *Counterdirectional rotation and axial flow*

When the effects of rotation oppose those induced by the pressure-driven axial flow, the flow situation is more complicated: the secondary flows can be different in nature in various regions of the parameter space.

For small negative values of $Ta$, the situation again resembles flow in stationary curved ducts. As the magnitude of $Ta$ is increased, however, system rotation enhances the strength of the axial flow and decreases that of the secondary flow, and this ultimately leads to qualitative changes in flow characteristics. These are shown in figure 6 for $D = 100$ on the primary solution branch for two values of $Ta$; figure 2(*a*) is representative of behaviour at low $Ta$ for comparison. The secondary flow for larger $|Ta|$ still consists of a pair of counter-rotating vortices, but the fluid now moves from the outer wall of the tube to the inner through the central core and recirculates around the periphery of the pipe. In addition, the position of the maximum axial velocity is shifted towards the inner wall of the tube. With an increase in $D$ (figure 7), the familiar picture obtained in stationary systems is recovered.

The mechanism of the secondary flow reversal can be seen in figure 8, which shows

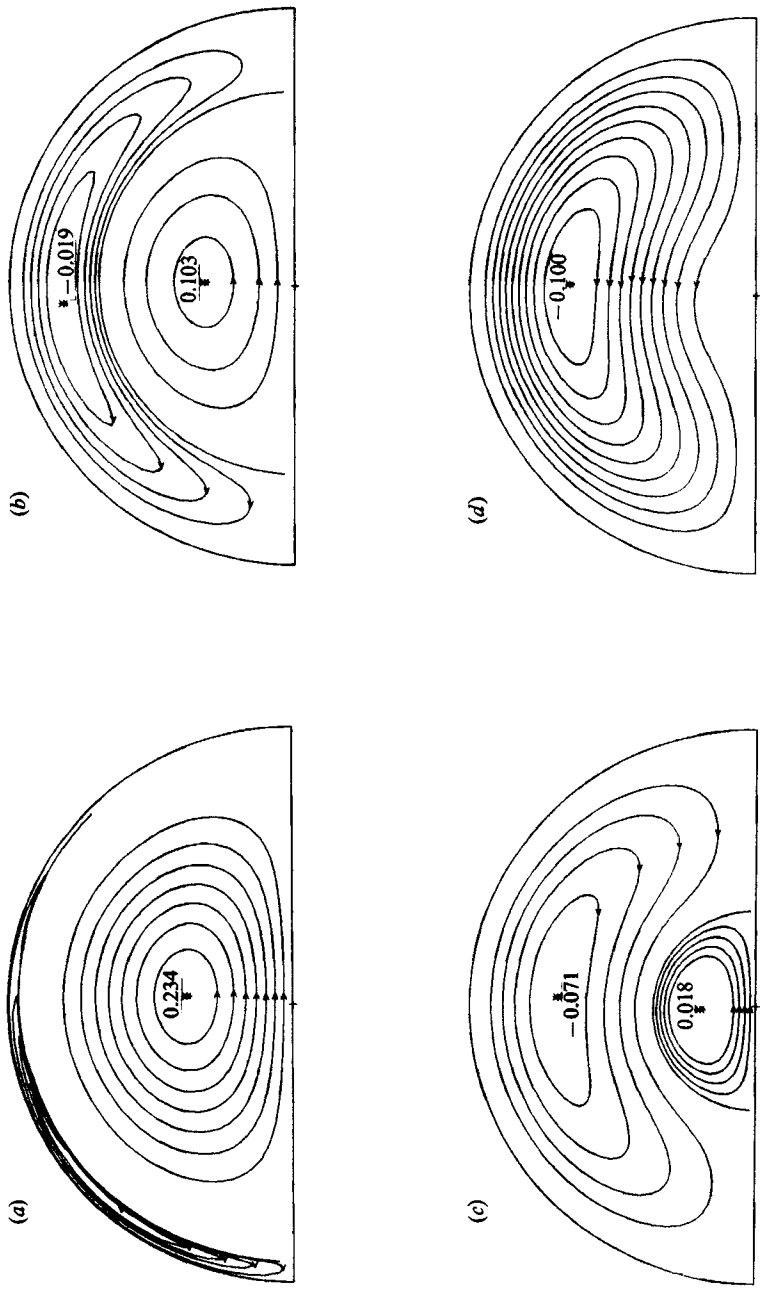


FIGURE 8. Secondary flow streamlines in the region of the secondary flow reversal, at $D = 100$. (*a*) $Ta = -25.641$, (*b*) $Ta = -29.412$, (*c*) $Ta = -32.258$, (*d*) $Ta = -33.333$.

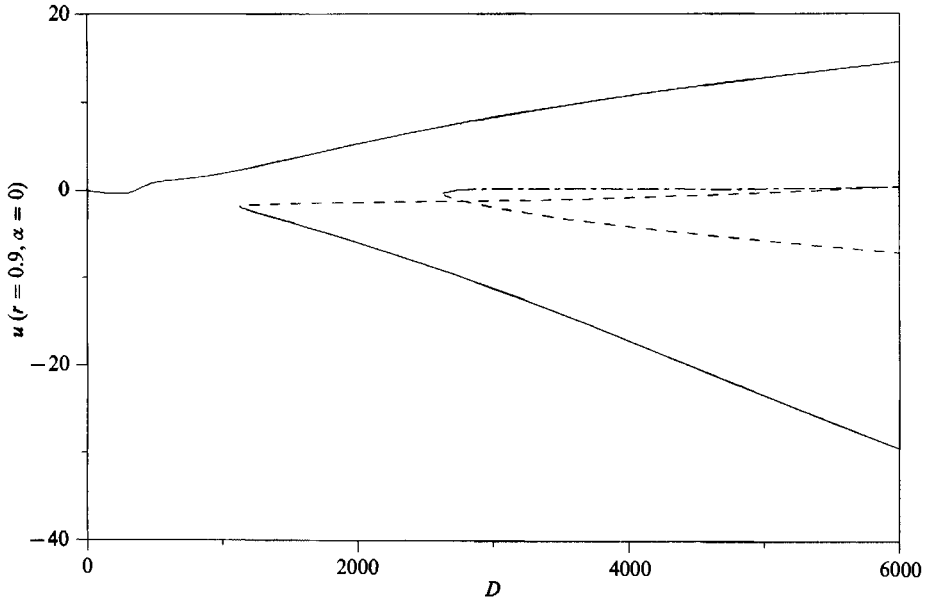


FIGURE 9. Bifurcation diagram at $Ta = -100$; key as for figure 5.

solutions in the neighbourhood of the transition for $D = 100$, obtained by continuation in $Ta$ with a small step. The results can be explained using qualitative arguments similar to those of Adler *et al.* (1982). With the axial flow opposing the spinning motion of the tube, there exists a parameter range where, overall, the effects of rotation neutralize those of the axial pumping. In this region, the fluid near the wall is left with the maximum net velocity relative to fixed axes. Centrifugal forces are then stronger near the wall of the tube and tend to throw the fluid outward, in a direction opposite to the familiar secondary flow pattern for stationary ducts. Hence a new vortex appears near the inner and lateral walls of the tube, squeezing the circulation due to the curvature of the system to the central portion of the tube. The original stable two-vortex family thus now exhibits a four-vortex structure which is qualitatively different from the four-vortex families encountered in stationary ducts. As the effects of rotation become stronger, the original circulation pattern is squeezed more and more to the pipe centre and finally vanishes, leaving a two-vortex circulation pattern again, but with the opposite direction of circulation.

The secondary flow reversal occurs at higher $D$ as $|Ta|$ is increased, and this is accompanied by qualitative changes. The apparent symmetry along the vertical centreline seen in figure 8 is due to the fact that the transition shown is for $D = 100$, where the secondary circulation arising from the effect of the pressure-driven axial flow is not very strong; this symmetry disappears at larger values of $D$. More significant, though, is the effect on the bifurcation structure. The bifurcation structure for $Ta = -100$ (figure 9) is the same as that seen previously: the reversal of the secondary flow direction for this rotational speed occurs smoothly, without the occurrence of any singular points. The existence in the original primary two-vortex solution of the type of four-vortex structure seen in figure 8 is restricted to a small, transitional range of the parameter space, in good agreement with the observations of Itō & Motai (1974).

For $|Ta| > 141.1$, however, the smooth transition in the bifurcation diagram

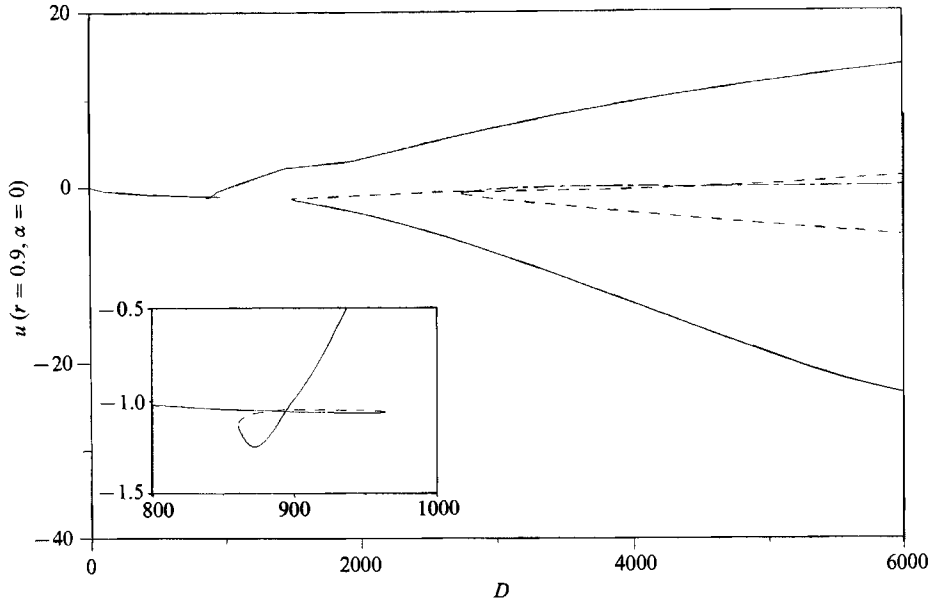


FIGURE 10. Bifurcation diagram at $Ta = -250$. Region around $D = 900$ is expanded in inset. Key as for figure 5.

| $Ta$ | $D_-$ | $D_+$ | $D_{app}$ | $D_{dis}$ |
|---|---|---|---|---|
| −100 | — | — | 350(+) | 600(+) |
| −125 | — | — | 395(+) | 1000(+) |
| −150 | 486.18 | 482.99 | 485(−) | 1450(+) |
| −200 | 709.42 | 664.54 | 700(−) | 2000(+) |
| −250 | 963.73 | 860.57 | 940(−) | 4900(+) |
| −500 | 2244.17 | 2084.85 | 2200(−) | >5000 |
| −750 | 3764.30 | 3544.66 | 3730(−) | >5000 |
| −1000 | 5618.36 | 5244.33 | >5000 | >5000 |

TABLE 2. Turning point development in the primary solution family. Negative rotation, secondary flow reversal region.

observed for $Ta = -100$ is replaced by a more complicated pattern through the appearance of a cusp in the primary solution branch, so that there is now an intervening unstable branch in the region of the secondary flow reversal. This is shown for $Ta = -250$ in figure 10. The appearance of the cusp is interesting in that it would give rise to abrupt transitions and hysteresis effects as parameters are changed in practice. Table 2 gives the positions of the turning points developing in the primary solution as a function of $Ta$, with $D_-$ denoting the first turning point, where the solution turns to become unstable, and $D_+$ the second, after which another stable branch exists. Although the turning points are associated with the reversal of the secondary flow, they do not correspond to the appearance and/or disappearance of the additional vortex. Table 2 also lists for comparison the approximate range over which the primary solution exhibits four-vortex structure, with $D_{app}$ denoting the appearance of the vortex arising from the curvature effects, i.e. the one observed

| $Ta$ | $D_1$ | $D_2$ |
|---|---|---|
| 0 | 955.73 | 2494.22 |
| −1 | 957.51 | 2503.06 |
| −10 | 972.67 | 2515.94 |
| −100 | 1131.77 | 2630.90 |
| −250 | 1494.61 | 2741.70 |
| −500 | 2295.14 | 2966.64 |
| −600 | 2861.61 | 3406.37 |
| −1000 | >5000 | >5000 |

TABLE 3. Turning points for the case of negative rotation

in stationary systems, and $D_{\mathrm{dis}}$ the disappearance of the vortex present in the rotation-dominated region. The sign (plus or minus) denotes whether the transition occurs on a stable or an unstable branch respectively. For the first two points in the table the flow reversal is smooth and these points are included in the table only for comparison of the four-vortex coexistence region. The Dean numbers associated both with the turning points and with vortex appearance and disappearance increase with increasing magnitudes of the Taylor number, as do the widths in the $D$ domain of the cusp and the coexistence region. Such interdependence of effects of Dean and Taylor numbers was also seen in the previous section (cf. figures 2 and 4) and is discussed further below.

Further increasing the magnitude of $Ta$ enhances the strength of the secondary flow, now with the new circulation pattern, and decreases the strength of the axial flow. This ultimately leads to the rotation-dominated region, where the effects of the pressure-driven flow are negligible compared to those of rotation, and the flow situation resembles that in the limit of very fast rotation as described in the previous section.

In addition to the primary solution, the other solutions discussed earlier remain as independent solutions, but the turning points are shifted towards larger $D$ as the effects of rotation are increased. The effects of the increased strength of rotation on these families are similar to those seen for the primary solution family. Table 3 shows the positions of the turning points of the two additional families as a function of the Taylor number. The values at high $|Ta|$ indicate that only the primary solution branch exists in the usual range of interest (up to $D = 5000$) for high rotational speeds. For small magnitudes of $Ta$ no flow reversal is observed in the flows belonging to the additional families, but as the effect of rotation becomes stronger, secondary flow reversal similar to that for the primary solution is observed. Figure 11 depicts a solution from the stable four-vortex solution for $Ta = -500$. The flow pattern is more complex: an additional circulation vortex appears near the inner wall, becoming weaker and smaller as $D$ is increased.

A simple criterion for estimating where the secondary flow reversal occurs can be obtained from a simplified analysis neglecting secondary flows. For small curvature, the axial velocity distribution can be approximated by the superposition of Poiseuille flow and solid-body rotation, from which the average axial velocity is

$$\langle W \rangle = \omega R + \frac{a^2 G}{8\mu}. \tag{6}$$

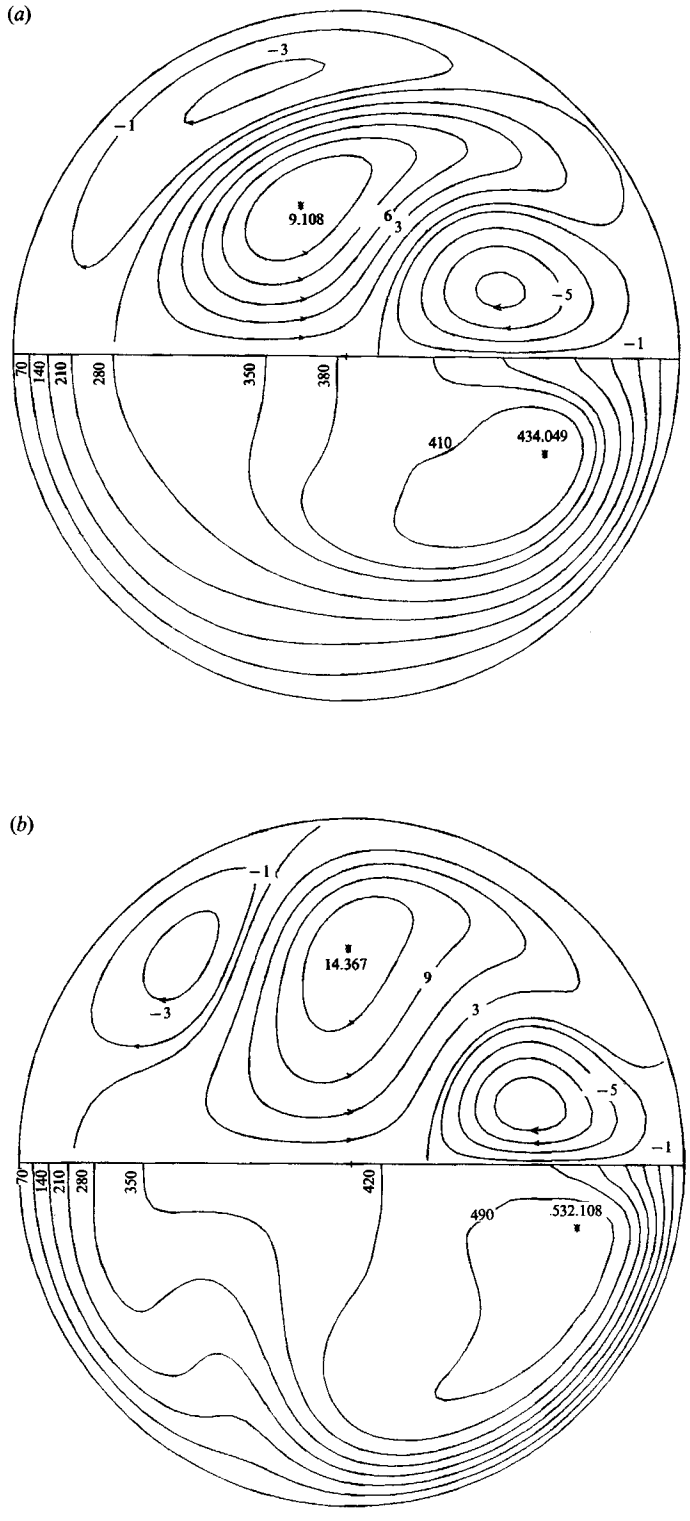


FIGURE 11. Secondary flow streamlines and axial velocity contours for stable four-vortex solution at $Ta = -500$. (*a*) $D = 3000$; (*b*) $D = 5000$.

| $Ta$ | Additional vortex appears | Original vortex disappears |
|---|---|---|
| −100 | −3.5 | −6.0 |
| −125 | −3.2 | −8.0 |
| −150 | −3.2 | −9.7 |
| −200 | −3.5 | −10.0 |
| −250 | −3.8 | −19.6 |

TABLE 4. Secondary flow reversal region. The parameter introduced in equation (7) is shown as a function of $Ta$.

If a zero mean axial flow is used as a measure of when the effects of rotation and pressure-driven flow balance each other, the criterion

$$\frac{D}{Ta} = -4 \tag{7}$$

is obtained as an estimate of the region where the secondary flow reversal should occur. If $D/Ta$, the Rossby number, is evaluated at the positions at which secondary flow reversal occurs, the results shown in table 4 are obtained. 'Original' refers to the vortex possible for small values of $D$, i.e. with circulation from the outer wall of the tube to the inner through the central core of fluid, and 'additional' to the one induced by the pressure-driven axial flow. Equation (7) is consistent in predicting the region where reversal of the secondary flow occurs, although the range of coexistence of the two solutions increases with increasing magnitudes of $Ta$. Because of use of Poiseuille flow in the approximation of the axial velocity profile, equation (7) is expected to be more accurate for small values of $D$. In fact Itō & Motai (1974), whose development was limited to small $D$, were the first to note the dependence of secondary flow reversal on the parameter $D/Ta$.

## 4. Concluding remarks

The results presented here appreciably extend the range of parameters for which flow in rotating curved tubes has been studied, especially as regards the bifurcation structure. The behaviour for codirectional rotation and axial flow is qualitatively the same as that in the absence of rotation, but for counterdirectional rotation and axial flow, a secondary flow reversal is possible, which may be accompanied by a new cusp in the bifurcation diagram at higher $|Ta|$. The existence of additional symmetric solutions may be investigated via the morphogenesis approach used in I; the relevant perfect problem is the combined Taylor–Dean situation of pressure-driven azimuthal flow between corotating cylinders (Daskopoulos & Lenhoff 1990). The effect of curvature, in equation (1) and, more generally, when the small-curvature assumption is relaxed, remains to be investigated, as do the possibility of asymmetric solutions and the stability to asymmetric disturbances.

The support of the National Science Foundation under grant CBT-8746050, including access to the Pittsburgh Supercomputing Center, is gratefully acknowledged.

## REFERENCES


ADLER, R. J., GORENSEK, M. B., LANDIN, M. E., MENON, M. M., PAPANU, J. S. & TROST, H. F. 1981 A new method of fine particle slurry fractionation. Paper presented at *ACS National Meeting, New York.*

ADLER, R. J., GORENSEK, M. B., MENON, M. M. & PAPANU, J. S. 1982 Periodic axial and secondary flow centrifugal separation. Paper presented at *AIChE Annual Meeting, Los Angeles.*

BARUA, S. N. 1954 Secondary flow in a rotating straight pipe. *Proc. R. Soc. Lond.* A **227**, 133–139.

BARUA, S. N. 1963 On secondary flow in stationary curved pipes. *Q. J. Mech. Appl. Maths* **16**, 61–77.

BATCHELOR, G. K. 1967 *An Introduction to Fluid Dynamics.* Cambridge University Press.

BENJAMIN, T. B. 1978 Bifurcation phenomena in steady flows of a viscous fluid. I. Theory. *Proc. R. Soc. Lond.* A **359**, 1–26.

BENTON, G. S. & BOYER, D. 1966 Flow through a rapidly rotating conduit of arbitrary cross-section. *J. Fluid Mech.* **26**, 69–79.

DASKOPOULOS, P. 1989 Flow in separations processes in rotating helically coiled tubes. Ph.D. thesis, University of Delaware.

DASKOPOULOS, P. & LENHOFF, A. M. 1989 Flow in curved ducts: bifurcation structure for stationary ducts. *J. Fluid Mech.* **203**, 125–148 (referred to herein as I).

DASKOPOULOS, P. & LENHOFF, A. M. 1990 The Taylor–Dean problem with co-rotating cylinders. *Z. Angew. Math. Phys.* (in press).

DEAN, W. R. 1927 Note on the motion of fluid in a curved pipe. *Phil. Mag.* (7) **4**, 208–223.

DEAN, W. R. 1928 The streamline motion of fluid in a curved pipe (second paper). *Phil. Mag* (7) **5**, 673–695.

DEAN, W. R. & HURST, J. M. 1959 Note on the motion of fluid in a curved pipe. *Mathematika* **6**, 77–85.

EUTENEUER, G.-A. & PIESCHE, M. 1978 Druckabfallmessungen in stationär rotierenden, gekrümmten Kanalstrecken mit quadratischem sowie kreisförmigem Durchflußquerschnitt. *Forsch. Ing.-Wes.* **44**, 53–56.

GREENSPAN, H. P. 1968 *The Theory of Rotating Fluids.* Cambridge University Press.

HART, J. E. 1971 Instability and secondary motion in a rotating channel flow. *J. Fluid Mech.* **45**, 341–351.

HOCKING, L. M. 1967 Boundary and shear layers in a curved rotating pipe. *J. Math. Phys. Sci.* **1**, 123–136.

ITŌ, H. & MOTAI, T. 1974 Secondary flow in a rotating curved pipe. *Rep. Inst. High Speed Mech.* **29**, 33–57.

ITŌ, H. & NANBU, K. 1971 Flow in rotating straight pipes of circular cross section. *Trans. ASME* D: *J. Basic Engng* **93**, 383–394.

JONES, J. R. & WALTERS, T. S. 1967 A note on the motion of a viscous liquid in a rotating straight pipe. *Z. Angew. Math. Phys.* **18**, 774–781.

JOSEPH, B. & ADLER, R. J. 1975 Numerical treatment of laminar flow in helically coiled tubes of square cross section. Part II. Oscillating helically coiled tubes. *AIChE J.* **21**, 974–979.

KELLER, H. B. 1977 Numerical solution of bifurcation and nonlinear eigenvalue problems. In *Applications of Bifurcation Theory* (ed. P. H. Rabinowitz), pp. 359–384. Academic.

KELLER, H. B. 1982 Continuation methods in computational fluid dynamics. In *Numerical and Physical Aspects of Aerodynamic Flows* (ed. T. Cebeci), pp. 3–13. Springer.

KHESHGI, H. S. & SCRIVEN, L. E. 1985 Viscous flow through a rotating square channel. *Phys. Fluids* **28**, 2968–2979.

LENNARTZ, J. W., GORENSEK, M. B. & ADLER, R. J. 1987 Separation of fine-particle dispersions using periodic flows in a spinning coiled tube. Part III: Batch fractionation experiments. *AIChE J.* **33**, 506–509.

LUDWIEG, H. 1951 Die ausgebildete Kanalströmung in einem rotierenden System. *Ing. Arch.* **19**, 296–308.

MANSOUR, K. 1985 Laminar flow through a slowly rotating straight pipe. *J. Fluid Mech.* **150**, 1–21.

MENON, M. M. 1984 Periodic centrifugal separations. M.S. thesis, Case Western Reserve University.

MIYAZAKI, H. 1971 Combined free and forced convective heat transfer and fluid flow in a rotating curved circular tube. *Intl J. Heat Mass Transfer* **14**, 1295–1309.

MIYAZAKI, H. 1973 Combined free- and forced-convective heat transfer and fluid flow in rotating curved rectangular tubes. *Trans. ASME* C: *J. Heat Transfer* **95**, 64–71.

MORI, Y. & NAKAYAMA, W. 1968 Convective heat transfer in rotating radial circular pipes. *Intl J. Heat Mass Transfer* **11**, 1027–1040.

PIESCHE, M. 1982 Experimente zum Strömungswiderstand in gekrümmten, rotierenden Kanälen mit quadratischem Querschnitt. *Acta Mechanica* **42**, 145–151.

PIESCHE, M. & FELSCH, K.-O. 1980 Experimental investigation of pressure loss in rotating curved rectangular channels. *Arch. Mech.* **32**, 747–756.

SPEZIALE, C. G. 1982 Numerical study of viscous flow in rotating rectangular ducts. *J. Fluid Mech.* **122**, 251–271.

VAN DYKE, M. 1975 Computer extension of perturbation series in fluid mechanics. *SIAM J. Appl. Maths* **28**, 720–734.

VAN DYKE, M. 1978 Extended Stokes series: laminar flow through a loosely coiled pipe. *J. Fluid Mech.* **86**, 129–145.

WINTERS, K. H. 1987 A bifurcation study of laminar flow in a curved tube of rectangular cross-section. *J. Fluid Mech.* **180**, 343–369.